Poly(thieno[3,4-*b*]furan), a New Low Band Gap Polymer: Experiment and Theory

Arvind Kumar,[†,§] Jayesh G. Bokria,[†,§] Zeki Buyukmumcu,[‡,§] Tanmoy Dey,[†] and Gregory A. Sotzing*[,†]

Department of Chemistry and the Polymer Program, Institute of Materials Science, University of Connecticut, Storrs, Connecticut 06269-3136, and Department of Chemistry, Erciyes University, Kayseri, Turkey

Received December 12, 2007; Revised Manuscript Received July 2, 2008

ABSTRACT: A new optically transparent, near-infrared-absorbing low energy gap conjugated polymer, poly(thieno[3,4-*b*]furan) (PT34bF), with promising attributes for photovoltaics is reported herein. PT34bF was prepared electrochemically, and upon redox cycling, doping was found to be anion dominant. The energy gap of the polymer was found to be 1.04 eV as calculated from the low-energy edge of the absorption spectrum of the neutral polymer at −0.6 V and 1.03 eV for the chemically neutralized polymer using hydrazine. The polymer is pale blue in the neutral form and a more transparent pale blue in the oxidized conducting state with photopic transmittances of 62% and 72% (ITO glass substrate not subtracted), indicating the possibility of application as a transparent conductor or an ion-storage layer for electronic devices. Density functional theory (DFT) calculations using B3PW91 hybrid functional have been carried out for possible connections between the three open α-positions. In addition to optimizing geometry, band structure properties such as band (energy) gaps, band widths, and effective masses were calculated for each connection. Calculations show that 4−6 connectivity is the most probable and dominant structure for the polymer resulting from T34bF, and the calculated energy gap of 1.01 eV for polymerization via this connection corresponds well with the experimentally observed value of 1.04 eV.

Introduction

The field of conjugated polymers (CPs) has been growing at a significant pace since the discovery of iodine-doped polyacetylene as a conducting polymeric material.[1] These polymers have enhanced material properties such as flexibility, low density, ease of processability, and thus a relatively low cost of production. Further, CPs offer large chemical structure variations, thereby providing a wider range of electrical and optical properties. They have therefore seen utility in varied fields like electrochromics,[2] volatile organic gas sensors,[3] nonlinear optics,[4] light-emitting diodes (LEDs),[5] energy storage batteries,[6] charge dissipation film,[7] protective coatings for corrosion prevention,[8] and photovoltaics,[9] to name a few. The electrical and optical properties of CPs mostly depend upon the energy gap (E_g, also known as the band gap) and is defined as the difference in energy between the highest occupied molecular orbital (HOMO) and lowest unoccupied molecular orbital (LUMO) levels, and there has been a great interest in the utility of low energy gap conjugated polymers as optically transparent electrodes and hole-injection layers for light-emitting diodes and photovoltaic devices.[10] By definition, low energy gap polymers (LEGP) are conjugated polymers having $E_g \leq 1.5$ eV,[11] with an absorption edge ≥600 nm in their neutral state. These unique materials have recently found applications in the field of photovoltaic devices,[9] electrochromic devices,[12] near-infrared applications,[13,14] and transistors.[15]

Although by strict definition poly(ethylenedioxythiophene) (PEDOT) ($E_g = 1.6-1.7$ eV[16]) is not a LEGP, it is widely used in the field, and a formulation with poly(styrenesulfonate) (PSS) is commercially available as Baytron-P by H.C. Starck. Because of its relatively high optical transparency and high stability in the conducting (oxidized) state, PEDOT has found varied applications in electronic and optoelectronic devices, with emphasis on its use in optically transparent electrodes and hole injection layers. The lowering of E_g of PEDOT vs poly(thiophene) has been attributed to the raising of the HOMO (with little expense to raising of LUMO) due to electron-rich oxygen atoms from the cyclic ethylenedioxy ring and reduction of sterics in the polymeric backbone allowing a more planar structure. LEGPs hold much promise as optically transparent conductors as the lowering of the energy gap results in a shift of the absorption spectrum out of the visible and into the near-infrared (NIR) region, thereby making them transparent to the naked eye. Out of the several methodologies to lower the energy gap, polymerization of fused heterocyclic monomers is one of the most promising ways to synthesize low energy gap polymers.

Wudl et al. reported the first low energy gap polymer,[17] poly(isothianaphtene) (PITN), by electropolymerizing isothianaphthene (ITN) and reported an energy gap of 1.0−1.2 eV. This low value of E_g was explained on the basis of the higher stability of the quinonoid form of thiophene since the benzene ring retained its aromaticity.[17,18] PITN was found to be environmentally unstable, thereby limiting its application, and thus various derivatives of PITN have been synthesized to improve the stability and relative processability, without compromising its energy gap.[19,20] In accordance with this methodology, thieno[3,4-*b*]thiophene (T34bT) wherein a thiophene ring is fused to another thiophene (instead of a benzene as in ITN) was prepared, and electrochemical polymerization of 2-decylthieno[3,4-*b*]thiophene[21,22] was reported with an energy gap of 0.92 eV; however, unsubstituted T34bT was not mentioned. Therefore, we prepared conjugated polymers from unsubstituted T34bT and demonstrated a very low energy gap of 0.85 eV for the electrochemically generated poly(thieno[3,4-*b*]thiophene) (PT34bT) from T34bT.[23] We have also reported aqueous dispersion polymerizations of T34bT to produce water-dispersible PT34bTs with band gaps ranging from 1.0 to 1.1 eV that are stable in water for over a year.[24] Furthermore, we have demonstrated that insoluble PT34bT prepared via oxidative chemical polymerization can be post-derivatized by sulfonation

* Corresponding author. E-mail: sotzing@mail.ims.uconn.edu.
† University of Connecticut.
‡ Erciyes University.
§ These authors contributed equally.

10.1021/ma702773e CCC: $40.75
Published on Web 09/17/2008

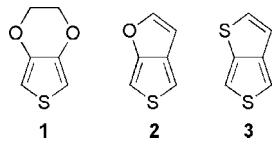

1 **2** **3**

Figure 1. Chemical structures of 3,4-ethylenedioxythiophene (**1**), thieno[3,4-*b*]furan (**2**), and thieno[3,4-*b*]thiophene (**3**).

to afford low band gap water processable polymer, and Langmuir−Blodgett films can be assembled via layer-by-layer deposition. This process offers a means to fine-tune the energy gap by carefully controlling the sulfonation level.[25] Simultaneous electropolymerization[26] of T34bT and EDOT to produce stable low band gap conjugated copolymers was also reported. Keeping in line with the same methodology, we communicated thieno[3,4-*b*]furan (T34bF), where now instead of a thiophene ring, as in T34bT, a furan ring is attached to another thiophene and was also a LEGP.[27] This new monomer bears resemblance to both EDOT and T34bT, as shown in Figure 1. The polymer, poly(thieno[3,4-*b*]furan (PT34bF), obtained from T34bF showed a very low energy gap of 1.04 eV as calculated from the onset of absorption and was in agreement with the theoretical value of 1.01 eV as found by DFT calculations assuming a 4−6 connection between consecutive T34bF repeat units in the polymer. We expand upon our initial communication with respect to both the experimental and theoretical aspects of poly(thieno[3,4-*b*]furan), including a detailed characterization and molecular calculations and its potential application in the emerging field of organic photovoltaics.

Experimental Section

Chemicals. Furfuryl mercaptan, ethylmagnesium bromide (1 M solution in THF), and propargyl chloride were purchased from Aldrich, whereas methyl choloroformate, copper chromite, and 2,3-dichloro-5,6-dicyano-*p*-benzoquinone (DDQ) were purchased from ACROS Chemicals and used without further purification. 3,6-Di(pyridine-2′-yl)-*s*-tetrazine (DPT) was prepared according to a literature procedure.[28] Acetonitrile (ACN), dichloromethane (DCM), toluene, and tetrahydrofuran (THF) were purchased from Fisher and purified prior to use. Under an inert atmosphere, ACN and DCM were dried over calcium hydride and toluene over sodium, and THF was dried over benzophenone ketyl and potassium and freshly distilled before use. Quinoline was purchased from ACROS Chemicals and purified by washing with HCl (10% aqueous solution) followed by NaOH (10% aqueous solution) before distilling it over zinc dust under a nitrogen atmosphere. The electrolytes—lithium triflate, tetrabutylammonium hexafluorophosphate, and tetrabutylammonium tetrafluoroborate—were purchased from Aldrich and used as received. Tetrabutylammonium perchlorate was synthesized by adding perchloric acid dropwise to the ice-cold aqueous solution of tetrabuylammonium bromide while stirring. (*Caution*: *perchloric acid and organic perchlorates are potentially explosive and should not be mixed with organics*; *proper precautions must be taken for handling and disposing these materials and waste generated thereof.*) The precipitate was filtered, dried, recrystallized from ethanol, and dried under vacuum for 24 h before use.

Instrumentation. A Bruker 400 or 500 FT-NMR spectrometer was used to record ^{1}H and ^{13}C nuclear magnetic resonance (NMR) spectra using tetramethylsilane (TMS) as an internal reference. Chemical shifts are reported as ppm downfield from TMS and peak multiplicities are reported as br = broad signal, s = singlet, d = doublet, t = triplet, q = quartet, dd = doublet of doublets, and m = multiplet. A CH Instruments CHI 400 potentiostat was used for all electrochemical studies, and a Perkin-Elmer Lambda 900 UV−Vis−NIR spectrophotometer equipped with UV win laboratory software was used for all optical studies. A Tencor Step 200 optical profilometer was used to determine the polymer film thickness where necessary. Fourier transform infrared (FTIR) data were acquired using using a Niclotet Magna 560 FTIR spectrometer operating in transmission mode. Elemental analysis was performed on a vario MICRO Elementar, calibrated with sulfanilamide standard and equipped for simultaneous detection of C, H, N, and S, while O was obtained by subtraction.

2-[(Prop-2′-ynylthio)methyl]furan.[32] Sodium hydride (3.0 g, 125 mmol) was added into a vacuum-dried three-neck flask containing 300 mL of anhydrous THF at 0 °C. Furfuryl mercaptan (13.77 g, 121 mmol) was added dropwise via syringe to the sodium hydride dispersion in THF, and reaction was allowed to continue at 0 °C for 1 h. At this stage, the reaction mixture is desired white in color. Propargyl chloride (9.5 mL, 125 mmol) was then added dropwise into the reaction flask and stirred for 4 h at 0 °C and another 6 h at room temperature. Higher temperatures during the NaH step leads to dark brown coloration, and addition of propargyl chloride resulted in the formation of 2-((prop-1-ynylthio)methyl)-furan and 2-((propa-1,2-dienylthio)methyl)furan in the ratio of 95:5 as the final product instead of the desired 2-[(prop-2′-ynylthio)-methyl]furan. 100 mL of water was carefully added to the reaction, and solution was concentrated by evaporating THF and unreacted propargyl chloride under vacuum. Diluting with diethyl ether and washing with 10% aqueous KOH removed any remaining furfuryl mercaptan. The organic layer was collected, dried over anhydrous $MgSO_4$, and concentrated using a rotavapor to get the product as dark yellow liquid in 68% average yield and was ∼98% pure by GC and ^{1}H NMR. GC-MS (*m*/*z*): 152 (M), 81 (100). ^{1}H NMR: δ 7.31 (dd, J = 1.7, 0.7 Hz, 1H), 6.27 (dd, J = 3.0, 1.9 Hz, 1H,), 6.17 (d, J = 2.75, 1H), 3.85 (s, 2H), 3.14 (d, J = 2.6 Hz, 2H), 2.25 (t, J = 2.5 Hz, 1H). ^{13}C NMR: 150.9, 142.4, 110.5, 108.1, 79.6, 71.5, 27.5, 18.5. FTIR (liquid film): 3294, 3146, 3117, 2949, 2911, 1502, 1409, 1250, 1234, 1150, 1071, 1011, 936, 885, 810, 740, 699, 645, 598 cm^{-1}. Elemental Analysis, calculated for C_8H_8OS: C, 63.07; H, 5.25; O, 10.51; S, 21.02. Found: C, 60.17; H, 5.18; O, 16.46; S, 18.06.

Methyl 4-(Furan-2′-ylmethylthio)but-2-ynoate.[32] In a vacuum-dried three-neck round-bottom flask, 2-[(prop-2′-ynylthio)methyl]-furan (11.0 g, 72 mmol) was taken along with 300 mL of anhydrous THF. After cooling the solution to 0 °C, 1 M ethylmagnesium bromide solution (99.8 mL, 99.8 mmol) was added dropwise under a nitrogen atmosphere. Reaction was continued at 0 °C for 2 h and at room temperature for 30 min. After cooling to 0 °C for 30 min, methyl chloroformate was added, and reaction was continued at room temperature for 8 h. The reaction was quenched by adding water and concentrated using a rotavapor. Diethyl ether and aqueous ammonium chloride solution were added to the concentrated mixture, and organic layer washed with copious amounts of water, dried over anhydrous $MgSO_4$, and concentrated using a rotavapor. The product obtained was ≥96% pure with an average yield of 80%. GC-MS (*m*/*z*): 210 (M), 81 (100). ^{1}H NMR: 7.38−7.33 (m, 1H), 6.31−6.20 (m, 2H), 3.87 (m, 2H), 3.71 (s, 3H), 3.27 (s, 2H). ^{13}C NMR: 153.9, 150.3, 142.7, 110.6, 108.5, 84.1, 74.8, 52.8, 27.8, 18.7. FTIR (liquid film): 3148, 3120, 2954, 2331, 2237, 1749, 1716, 1503, 1435, 1409, 1263, 1150, 1074, 1011, 937, 818, 749 cm^{-1}. Elemental Analysis, calculated for $C_{10}H_{10}O_3S$: C, 57.07; H, 4.75; O, 22.83; S, 15.20. Found: C, 56.43; H, 4.64; O, 21.31; S, 17.54.

Methyl 4,6-Dihydrothieno[3,4-*b*]furan-3-carboxylate.[32] Methyl 4-(furan-2′-ylmethylthio)but-2-ynoate (2.0 g, 9.52 mmol) was taken in a dry one-neck flask along with the 3,6-di(pyridine-2′-yl)-*s*-tetrazine (DPT) (2.4 g, 10 mmol) and toluene (100 mL). The reaction mixture was refluxed at 120 °C for 24 h under a nitrogen atmosphere and then cooled to room temperature before evaporating the toluene using a rotavapor. 100 mL of diethyl ether was added to the crude mixture and filtered. The filtrate was washed with dilute HCl followed by water, and the organic layer (free of any unreacted DPT) was dried over anhydrous $MgSO_4$, filtered, and concentrated using a rotavapor. The desired product was obtained in 54% yield with no indication of methyl 4-(furan-2′-ylmethylthio)but-2-ynoate present as evident by GC-MS and ^{1}H NMR. No further purification was performed, and the crude was subjected to the next step. GC-MS (*m*/*z*): 184 (M, 100). ^{1}H NMR: 7.90 (s, 1H), 3.98 (m, 4H), 3.80 (s, 3H). ^{13}C NMR: 163.2, 156.6, 151.9, 124.6, 117.5, 51.5,

28.5, 28.0. FTIR (KBr pellet): 3131, 3064, 2949, 2926, 1716, 1541, 1434, 1422, 1323, 1273, 1203, 1115, 1103, 1003, 810, 767 cm^{-1}. Elemental Analysis, calculated for $C_8H_8O_3S$: C, 52.11; H, 4.34; O, 26.06; S, 17.37. Found: C, 51.45; H, 4.30; O, 27.39; S, 16.86.

4,6-Dihydrothieno[3,4-*b*]furan-3-carboxylic Acid.[32] The crude methyl 4,6-dihydrothieno[3,4-*b*]furan-3-carboxylate (1.0 g) was refluxed in 200 mL 10% aqueous NaOH solution. After 6 h under a nitrogen atmosphere, the reaction mixture was cooled to room temperature and washed with diethyl ether. The basic aqueous layer was acidified by dilute HCl to precipitate the desired product. After filtration, the precipitate was thoroughly washed with water and dried overnight under vacuum at 70 °C. The product was >98% pure in 85% yield. GC-MS (*m*/*z*): 170 (M, 100). ^{1}H NMR: 12.81 (br, 1H), 8.21 (s, 1H), 3.95 (dd, J = 3.6, 3.1 Hz, 2H), 3.87 (dd, J = 3.5, 3.0 Hz, 2H). ^{13}C NMR: 167.6, 156.4, 153.2, 124.7, 116.7, 28.5, 28.0. FTIR (KBr pellet): 3175, 1685, 1541, 1436, 1399, 1290, 990, 921, 784 cm^{-1}. Elemental Analysis, calculated for $C_7H_6O_3S$: C, 49.35; H, 3.52; O, 28.20; S, 18.80. Found: C, 50.71; H, 3.80; O, 27.38; S, 17.90.

4,6-Dihydrothieno[3,4-*b*]furan.[32] 4,6-Dihydrothieno[3,4-*b*]furan-3-carboxylic acid (0.9 g, 5.3 mmol), copper chromite (0.183 g, 0.58 mmol), and freshly purified quinoline (10 mL) were taken in a dry one-neck flask and heated at 210 °C for 1 h under a nitrogen atmosphere. After cooling the reaction mixture to room temperature, diethyl ether (50 mL) was added and washed with aqueous $NaHCO_3$ solution to remove any unreacted acid followed by dilute HCl wash to remove quinoline. After washing with water, the organic layer was dried using anhydrous $MgSO_4$, filtered, and concentrated to obtain the desired product in 70% yield and used as such for the next step. GC-MS (*m*/*z*): 126 (M, 100). ^{1}H NMR: 7.38 (d, J = 1.4 Hz, 1H), 6.26 (d, J = 1.5 Hz, 1H), 3.95 (dd, J = 3.1, 3.6 Hz, 2H), 3.84 (dd, J = 3.3, 3.7 Hz, 2H). ^{13}C NMR: 155.0, 147.5, 124.6, 108.4, 28.5, 28.3. FTIR (liquid film): 3240, 2960, 2923, 2852, 2360, 2343, 1732, 1596, 1455, 1383, 1260, 1096, 1019, 802, 410 cm^{-1}. Elemental Analysis, calculated for C_6H_6OS: C, 57.06; H, 4.75; O, 12.68; S, 25.36. Found: C, 55.39; H, 5.23; O, 18.05; S, 20.38.

Thieno[3,4-*b*]furan.[32] 4,6-Dihydrothieno[3,4-*b*]furan (0.16 g, 1.27 mmol) and anhydrous methylene choride (10 mL) were taken in a dry three-neck flask and cooled the solution to 0 °C before adding DDQ (0.3 g, 1.32 mmol). The reaction mixture was stirred at 0 °C for 30 min and then passed through the silica. After evaporating the solvent, the product was purified by column chromatography using methylene chloride as an eluent. The purified product was obtained in 60% yield. GC-MS (*m*/*z*): 124 (M), 45 (100). ^{1}H NMR: 7.58 (d, J = 2.4 Hz, 1H), 6.92 (d, J = 2.5 Hz, 1H), 6.74 (d, J = 2.1 Hz, 1H), 6.41 (d, J = 2.0 Hz, 1H). ^{13}C NMR: 156.8, 153.0, 134.8, 107.1, 103.0, 94.9.

Electrochemistry. A three-electrode electrochemical cell was used for all the electrochemistry experiments using Ag/Ag^+ (nonaqueous) reference electrode which consisted of Ag wire dipped in 0.01 M $AgNO_3$ in 0.01 M $TBAPF_6$/acetonitrile inside a glass tube fitted with a Vycor tip. The reference electrode was calibrated to be 0.445 V vs normal hydrogen electrode (NHE) using ferrocene−ferrocenium redox. A 0.5 in. × 1 in. platinum flag was used as a counter electrode while Pt (2 mm diameter), Au (2 mm diameter), or vitreous C (3 mm diameter) button electrodes were used as working electrode. All polymerization experiments were done by using 0.01 M T34bF solution in 0.1 M electrolyte solution in acetonitrile, and the polymer electrochemistry was performed in the corresponding electrolyte solution (without monomer) used for polymerization. The electrolytes used for this study were tetrabutylammonium perchlorate, tetrabutylammonium hexafluorophosphate, tetrabutylammonium tetrafluoroborate, and lithium triflate.

EQCM Studies. Polished quartz crystals having resonant frequency of ~7.995 MHz were purchased from International Crystal Manufacturing. The crystals had a 0.201 in. diameter, 1000 Å thick gold key electrode with a 100 Å chromium underlay on either side of the crystal. The leads for electrical contact were sealed away from the solution. All the experiments were performed using a 1 cm^2 platinum flag as the counter electrode and a nonaqueous Ag/Ag^+ reference electrode. The polymer was deposited onto polished gold-coated quartz crystals from 0.01 M monomer solution in 0.1 M electrolyte/ACN by applying a potential of 1.25 V (vs Ag/Ag^+) for 5 s and then stepping to −1.0 V (vs Ag/Ag^+). It was then washed thoroughly with acetonitrile and dried before taking the electrochemical measurement in a monomer free electrolyte solution. TBAP, $TBAPF_6$, and $TBABF_4$ were used as an electrolyte for this study, and it should be noted that the electrochemical characterization was performed using the same electrolyte as used for electrochemical polymerization. The experiments were repeated at least 10 times for statistical reasons, and less than 1% error was observed.

Optoelectrochemical Measurement. ITO-coated glass was purchased from Delta Technologies and precleaned by sonication for optoelectronic studies. All the experiments were performed using polymer-coated ITO glass as working electrode in a three-electrode cell. Polymer, PT34bF, films onto ITO-coated glass were obtained from 0.01 M T34bF solution in 0.1 M TBAP/ACN solution by applying the +1.25 V (vs Ag/Ag^+) for 5 s using chronocoulometry. Polymer films were washed with acetonitrile and dried before using it as a working electrode for optical studies. Another ITO glass was used as counter electrode and Ag/Ag^+ (nonaqueous) as a reference electrode. All the electrodes were assembled in a glass cuvette and connected to a CHI 400 potentiostat. The cuvettes are placed inside the spectrophotometer to observe the in situ optical properties while changing the potential at working electrode using the potentiostat.

Conductivity Measurements. PT34bF was synthesized electrochemically on an ITO glass working electrode by using a constant potential of 1.25 V vs nonaqueous Ag/Ag^+ reference using 0.01 M T34bF in 0.1 M TBAP/ACN solution. The deposited PT34bF was washed well with ACN, carefully removed from the electrode, and treated with hydrazine to obtain the neutral form. The procedure was repeated multiple times to obtain 55 mg of polymer powder, dried in vacuum, and pressed into a disk of 1.2 cm diameter in a mold using a pressure of 57 kpsi. A four-point collinear array was used for conductivity measurement using a Keithley Instruments 224 constant current source and a 2700 multimeter. Conductivity was measured by applying current to two outer leads while measuring the potential between two inner leads and using the equation $\sigma = lI/twV$, where σ is the conductivity in units of S/cm, l is the distance between the two inner leads in centimeters, I is the current in amps, w is the width of the film in centimeters, t is the film thickness in centimeters, and V is the potential in volts. The PT34bF pellet was kept in iodine chamber for 30 min to obtain the iodine-doped form. We note that humidity was 60% with a room temperature of 25 ± 2 °C during all measurements.

Theoretical Studies. The Gaussian 03 program package[29] was used to study PT34bF having different repeat unit connectivities and details of the periodic boundary conditions (PBC) routine used to study several properties of periodic structures such as polymers are reported elsewhere.[30] The number of k-points for the band structure may be fixed by hand, and the default option of Gaussian wherein the number of the points is determined depending on the one-dimensional cell size was preferred. Geometry of the repeating unit of an infinite polymer chain has been optimized using the program default, redundant internal coordinates. The Becke three-parameter hybrid functional with the nonlocal correlation provided by Perdew/Wang 91 (B3PW91)[31] of density functional theory (DFT) with the basis set 6-31g(d,p) was used for restricted optimizations. In the previous study,[27] the dihedral angles were left free to vary during optimization and structures had very small deviations from planarity. In this study, however, based on energy scans between two monomer planes with varying torsional angles, the rings of repeating units were forced to be planar and dihedral angles were frozen at 0° and 180° during optimization.

Results and Discussion

Monomer Synthesis and Characterization. Thieno[3,4-*b*]furan (T34bF) was synthesized by modifying the reported procedure[32] and is shown in Figure 2. Modifications of the

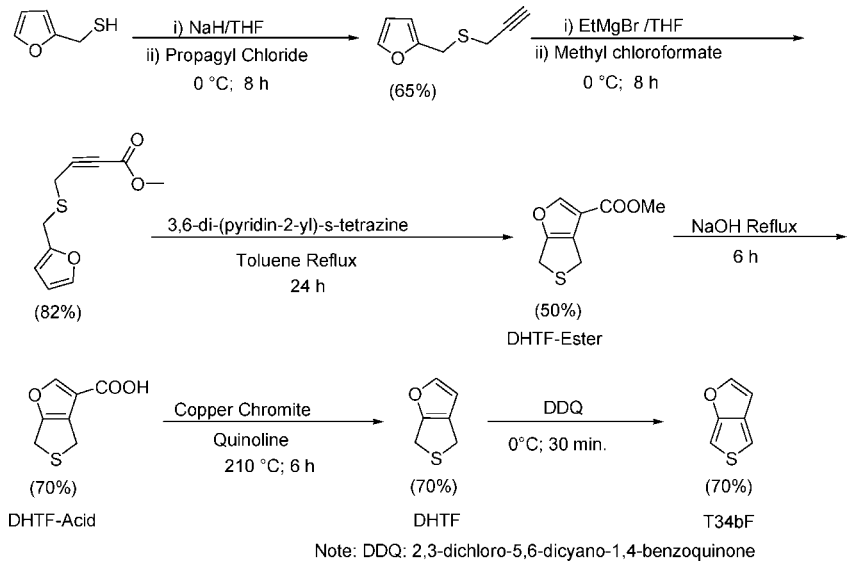

Figure 2. Synthesis of thieno[3,4-*b*]furan (T34bF).

reaction conditions were necessary for the synthesis and were in steps 1 and 6. The first step of the reaction was carried out at 0 °C instead of 25 °C as reported in the literature; higher temperatures resulted in the formation of 2-((prop-1-ynylthio)-methyl)furan and 2-((propa-1,2-dienylthio)methyl)furan in the ratio of 95:5 as the final product instead of 2-[(prop-2′-ynylthio)methyl]furan. The last (sixth) step was carried out at 0 °C, and not the reported 25 °C, as at this temperature an insoluble dark greenish-blue material formed, possibly as a result of the oxidative polymerization of the product, T34bF, by DDQ. Modified work-up protocol is also reported that reduces the time for synthesis, reduces cost, and improves scale-up. Time, labor, material, and environmentally expensive purification steps such as chromatography, distillation, and recrystallization were mostly eliminated. Our procedure required only a brief dry flash column after the last synthetic step of the reaction scheme and not purification at each step as in the case of previously reported procedure. T34bF was characterized by using ^{1}H NMR, ^{13}C NMR, and GC-MS, and results were found in accordance with the literature.[32] ^{1}H and ^{13}C NMR peak assignments were further confirmed by coupling between C atoms or C and H atoms via heteronuclear multiple bond correlation (HMBC) and heteronuclear multiple-quantum coherence (HMQC) NMR techniques and found to be consistent with that reported[32] by Moursounidis and Wege.

Poly(thieno[3,4-*b*]furan), PT34bF: Electrochemical Synthesis and Characterization. The polymer of T34bF, namely PT34bF, was prepared via electrochemical polymerization of 0.01 M T34bF in a 0.1 M electrolyte solution using acetonitrile (ACN) as the solvent using cyclic voltammetry. Various working button electrodes (platinum, gold, and vitreous carbon) in the presence of different electrolytes such as tetrabutylammonium hexafluorophosphate ($TBAPF_6$), tetrabutylammonium tetrafluoroborate ($TBABF_4$), tetrabutylammonium perchlorate (TBAP), and lithium triflate (LiTrif) were used for the electrodeposition. A typical cyclic voltammogram of the electropolymerization is shown in Figure 3, where a Pt button working electrode was used in the presence of $TBABF_4$/ACN electrolyte solution in a three-electrode electrochemical cell configuration containing Pt flag as a counter electrode and a nonaqueous Ag/Ag^+ as reference electrode. The reference electrode was calibrated before the electrochemical experiment using a 10 mM ferrocene standard in the appropriate electrolyte and calculated to be 0.445 V vs NHE.

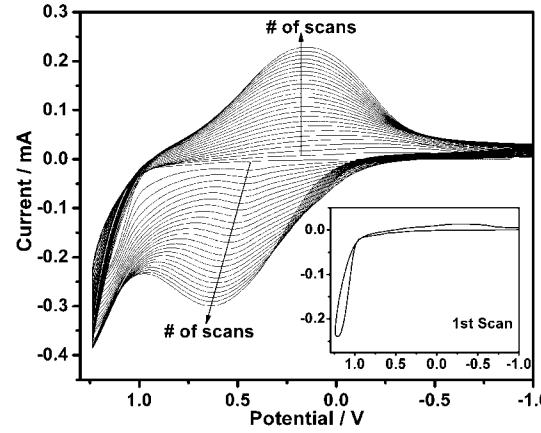

Figure 3. Electrochemical polymerization of 10 mM thieno[3,4-*b*]furan in 0.1 M $TBABF_4$/ACN at a scan rate of 100 mV/s using platinum working electrode. Twenty-five cyclic voltammograms are shown, with the first CV scan shown in the inset. Potentials are reported vs Ag/Ag^+ nonaqueous reference electrode (0.445 V vs NHE).

The first CV scan (shown in the inset of Figure 3) showed the onset of monomer oxidation at a potential of 0.96 V (vs Ag/Ag^+ reference) with a diffusion-limited peak at 1.21 eV corresponding to the oxidation of T34bF to its radical cation and thereafter coupling to form PT34bF. These values place T34bF at approximately the same potentials as EDOT[33,34] and T34bT.[23] The low oxidation potential of T34bF implies avoidance of overoxidation of the polymer formed during electrochemical polymerization, thereby negating the undesirable side reactions. Upon scanning in the cathodic direction, a broad reduction process is observed, corresponding to the reduction of the oxidized form of PT34bF deposited onto the working electrode during the previous anodic scan. During the second CV scan, a new oxidation process is observed at a lower oxidation potential with an onset at −0.42 V, peaking at 0.4 V, indicating the oxidation of a more conjugated species formed during the first CV scan.

On going further in the anodic direction, the current response corresponding to the oxidative polymerization of T34bF increases, indicating the deposition of more PT34bF onto the working electrode. This was further confirmed by the increase in the current response corresponding to the reduction of oxidized form of PT34bF to its neutral form and vice versa.

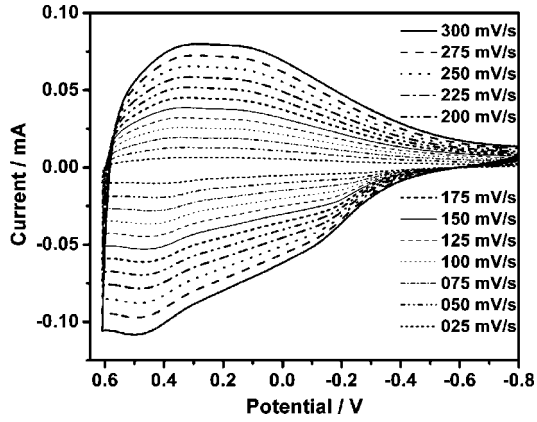

Figure 4. CV scans of polymer, PT34bF, deposited onto gold button electrode at different scan rates varying from 25 to 300 mV/s with an interval of 25 mV/s in 0.1 M $TBABF_4$/ACN electrolyte solution (A). Potential reported vs Ag/Ag^+ nonaqueous reference electrode (0.445 V vs NHE).

This increase in reduction and oxidation current during successive CV scans indicates the increase in the amount of electroactive material, viz. conducting polymer PT34bF on the electrode during each scan. Further, PT34bF was found to be stable in the potential window of −1.0 and +1.25 V as evident from 25 CV scans shown in Figure 3. Careful analysis of the CV shows that the peak position for the oxidation of PT34bF shifted by 0.2 V from 0.4 V to 0.6 V after 24 CV scans, and this may be attributed to the increase in the film thickness of conductive polymer deposited onto the electrode that slows the movement of ions through the polymer matrix during redox switching.

The electrochemical behavior of T34bF and PT34bF obtained thereof was investigated using different electrode−electrolyte combinations and was found to be independent of these variables. Irrespective of the choice of electrolyte and electrode, the onset of monomer oxidation was observed at 0.94 ± 0.02 V (vs Ag/Ag^+ nonaqueous reference). The diffusion-limited peak of monomer oxidation attributed to the oxidative polymerization of T34bF was observed at 1.24 ± 0.03 V (vs Ag/Ag^+ nonaqueous reference).

Scan Rate Dependency and Redox Switching of PT34bF. The polymer PT34bF was deposited on a gold working electrode using cyclicvoltammetry in a three-electrode cell. After electrodeposition, the Au button was removed and washed thoroughly with ACN. The polymer redox behavior was investigated in a monomer free electrolyte solution using the same electrolyte as that used for electrochemical polymerization while varying scan rates and is shown in Figure 4. The scan rate was varied from 25 to 300 mV/s with 25 mV/s increments. The linear increase of the redox current response with increase in scan rate fits the modified Randles−Sevcik equation and indicates that the electroactive species, conductive polymer PT34bF, is surface bound and adhered onto the electrode surface. CV of the polymer (in a monomer free electrolyte bath) showed a similar broad oxidation process with an onset at −0.42 V as that observed during electrochemical polymerization on Pt button. The oxidation peak was observed at 0.49 V with a distinct shoulder at −0.12 V and has been assigned to the oxidative conversion of neutral PT34bF to its doped (oxidized) form. On scanning in the cathodic direction, a broad reduction process was observed, corresponding to the reduction of oxidized PT34bF to its neutral form. To investigate the redox stability of PT34bF, the polymer was electrochemically switched 500 times in double-potential steps between its neutral (−0.5 V) and oxidized state (+0.6 V) in monomer free 0.1 M electrolyte solution in ACN. Despite the fact that this experiment was performed in ambient laboratory conditions with unoptimized experimental conditions, only ∼10% decrease in charge was observed using all four electrolyte solutions, indicating a high switching stability of PT34bF under ambient conditions.

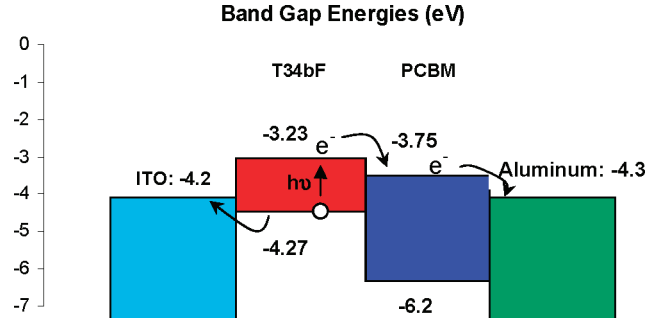

Figure 5. Band levels (in eV vs vacuum) of a device based on T34bF and PCBM and movement of the electron (e^-) and hole (o) created as a result of near-IR absorption.

Energy Levels. The HOMO level of PT34bF was calculated from cyclic voltammogram (CV) measurements vs ferrocene,[35] and since the band gap is known, the LUMO level found. The experimentally found energy levels for PT34bF agree with the theoretically calculated ones (vide infra). Figure 5 shows the band levels of PT34bF and PCBM along with the work functions of ITO[36] and aluminum. It is evident that the HOMO matches with the work function of ITO, while the LUMO matches with the acceptor level of PCBM. This implies that upon light absorption (in the near-infrared region, based on the band gap of PT34bF) effective splitting of the generated photoexciton can be achieved, and the electrons and holes can continue toward the cathode and anode, respectively. Further, since the HOMO level and the ITO work function are so close in energy, the Schottky barrier for hole injection would be minimized, and the need for a hole injection layer could possibly be erased.

Rate of Polymerization, Percent Ion Transport, and Doping Level. Concurrent chronogravimetry and chronocoulometry using an electrochemical quartz crystal microbalance (EQCM) were performed in order to study the kinetics of polymerization and doping behavior. Thus, T34bF was polymerized onto a gold QCM crystal by applying a constant potential of 1.25 V (vs nonaqueous Ag/Ag^+ reference) for a duration of 3 s in 10 mM T34bF/ 0.1 M $TBABF_4$/ACN solution using a Pt flag counter. The change in mass and charge, as a function of time of the applied potential, is shown in Figure 6A, and upon holding the potential at 1.25 eV a corresponding increase in mass along with ejection of charge is observed, indicating electrodeposition of the polymer on the crystal. Therefore, in a period of 3 s, 1.98 μg of PT34bF (in oxidized state with associated counterions) deposited on the crystal, corresponding to a rate of deposition of 660 ng/s. The polymer was then converted into the neutral form by stepping the potential to −0.8 V for another 3 s, and the mass loss observed during dedoping was attributed to the movement of ions out of the polymer matrix. Similar behavior as shown in Figure 6 was observed upon using other electrolytes such as TBAP and $TBAPF_6$.

The percent ion transport during the dedoping process can be calculated from the change in mass and charge utilized to reduce the polymer to its neutral form using the following equation[26,37]

$$m_{\text{final}} = m_{\text{initial}} - X_{\text{an}}M_{\text{an}} + \left(\frac{Q}{F} - X_{\text{an}}\right)M_{\text{cat}} \qquad (1)$$

where m_{initial} and m_{final} represents the mass of the polymer deposited in the oxidized form associated with the counterion

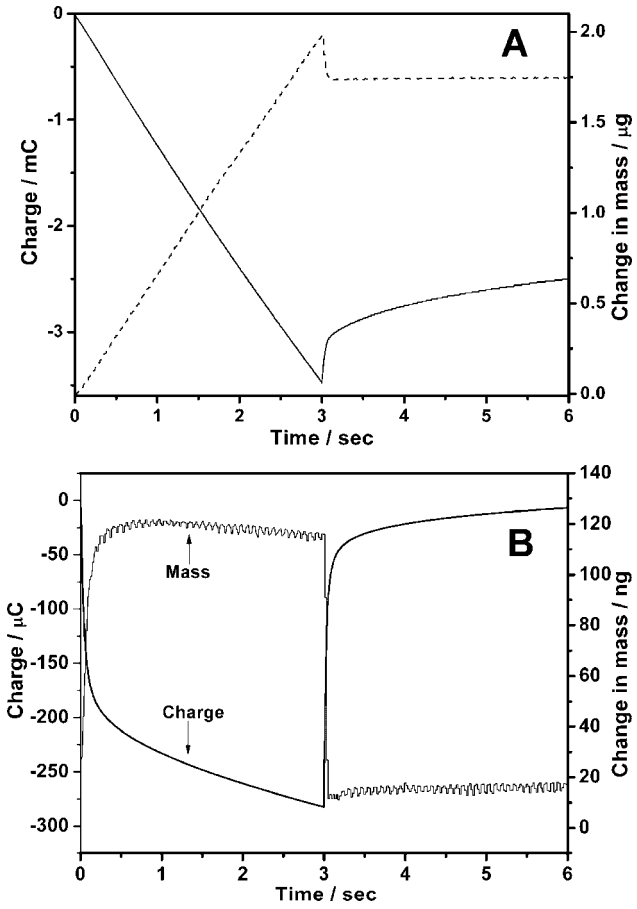

Figure 6. Chronocoulometry (solid line) and concurrent chronogravimetry (dashed line) during a two-step constant potential simultaneous polymerization of PT34bF in 10 mM T34bF/0.1 M $TBABF_4$/ACN using 1.25 V vs Ag/Ag^+ nonaqueous electrode (A) and during a single constant potential redox switch of PT34bF (B) in 0.1 M $TBABF_4$/ACN.

and mass of the neutral polymer obtained upon reduction, respectively, and X_{an} is the fraction of anions transported. M_{an} and M_{cat} are the molar masses of the anion and cation associated with electrolyte, respectively, Q is the charge consumed, and F is the Faraday constant = 96,485 C/mol.

The conducting polymer was switched between its redox states several times, and the percent ion transport was calculated under these stable ion flux conditions. This is critical to maintain a constant flux of ions during the redox process, and only then can ion transport mesurements be carried out. Thus, the quartz crystals, with polymer, were washed thoroughly with acetonitrile and switched at least 10 times between redox states by applying +0.6 and −0.6 V for 3 s each in the presence of monomer free electrolyte solution. During these pretreatment redox switches, the gravimetric and charge response was found to be stable. Figure 6B shows simultaneous chronocoulometry and chronogravimetry experiments on the PT34bF-coated quartz crystal in a 0.1 M $TBABF_4$/ACN solution. The polymer was first oxidized by holding it at +0.6 V for 3 s and then switched back to the neutral form by applying −0.6 V for another 3 s in one potential step. The change in mass and charge during this redox switching process in conjunction with the previous data for the charge and the corresponding polymer mass from Figure 6A were used to calculate the ion transport, and the results are shown in Table 1. As with the cyclic voltammetry studies, irrespective of the electrolytes used, PT34bF showed anion transport dominancy, with the highest value of 81.2% in case of $TBABF_4$ and lowest of 67.2% for $TBAPF_6$. The higher value

Table 1. Rate of Polymerization (R_p), Percent Anion (Tr_{an}) and Cation Transport (Tr_{cat}), and Percent Doping Level

electrolyte	R_p (nmol/s)	Tr_{an} (%)	Tr_{cat} (%)	doping level (%)
$TBABF_4$	3.0	81.2	18.8	29.9
TBAP	3.2	74.2	25.8	26.9
$TBAPF_6$	4.1	67.2	32.8	21.3

of anion transport in the case of $TBABF_4$ is attributed to the relatively smaller size of the BF_4^- anion.

The mass of neutral polymer deposited without any associated ions on the quartz crystal was calculated by subtracting mass of associated ions (determined from the ion transport data) from the final mass of neutral polymer with associated ions. The number of moles of repeat unit of polymer was obtained by dividing the neutral polymer mass by molar mass of the repeat unit. The rate of polymerization could then be reported in terms of moles of repeat units (monomers) consumed per second. The doping level was calculated by dividing the moles of charge consumed to dope the polymer by the moles of repeat unit present in the polymer deposited, and these results are also reported in Table 1. The doping level of 26.9% for PT34bF in TBAP/ACN solution was found to be similar to the reported value of 28.0% in the case of PT34bT obtained under similar experimental conditions[26] and corresponded to roughly one anion per three repeat units, consistent with those observed for conducting polymers.

Optical Characterization. A ~0.1 μm thick PT34bF film was galvanostatically deposited onto the working ITO-coated glass electrode and used to perform in situ optoelectrochemistry in a monomer free 0.1 M TBAP/ACN electrolyte solution. A three-electrode cell, with ITO glass as counter and nonaqueous Ag/Ag^+ as reference, was used, and a constant potential was maintained while simultaneously acquiring vis−NIR data. Figure 7 shows % transmittance of the PT34bF film on ITO at different potentials. At −0.6 V, the spectrum showed an onset of transmittance decay (or onset of absorption) at 1190 nm (1.04 eV) and corresponds to a $\pi-\pi^*$ transition of the neutral polymer and therefore the energy gap E_g of 1.04 eV. This value is essentially the same, within experimental error, as E_g = 1.03 eV found for the chemically reduced PT34bF by hydrazine and indicates the formation of a complete neutral form at −0.6 V. The % transmittance in the visible region increased as the potential increased from −0.6 to + 0.6 V along with a corresponding decrease in the NIR region due to absorbance of the polaronic and bipolaronic transitions resuling from the oxidized PT34bF, indicating the more transparent oxidized form of PT34bF at higher potentials. The color coordinates for PT34bF at different potentials were calculated using a CIE 1976

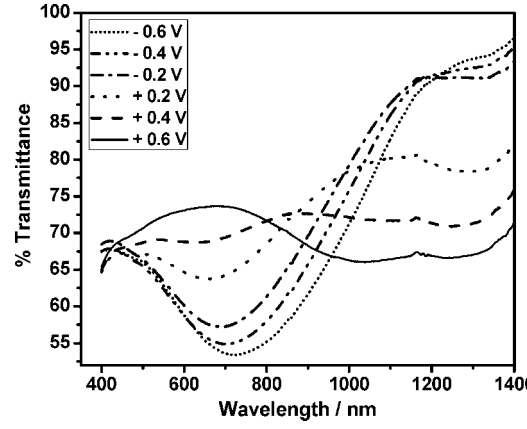

Figure 7. In situ spectroelectrochemistry of PT34bF deposited onto ITO-coated glass in 0.1 M TBAP/ACN. Potential reported vs nonaqueous Ag/Ag^+ reference electrode (0.445 V vs NHE).

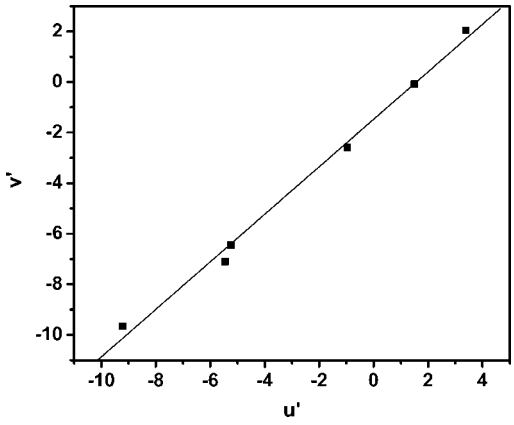

Figure 8. Transition of colors shown as CIE color space plots for PT34bF between −0.6 and +0.6 V (vs nonaqueous Ag/Ag^+) using 1976 CIE color standards.

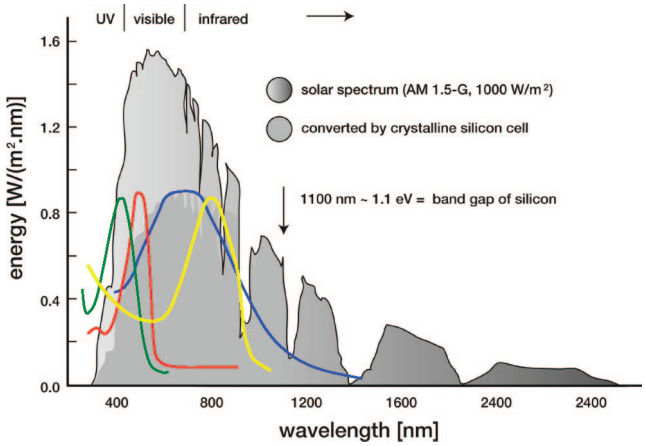

Figure 9. Solar spectrum material comparison. Curves were normalized for relative absorbance, but the peaks remain at their correct wavelengths (blue = thieno[3,4-*b*]furan, yellow = thieno[3,4-*b*]thiophene, red = MEH−PPV in acetone, green = poly(3-hexylthiophene)).

two-point standard observer, and the results are shown in Figure 8.

The absorption spectrum of PT34bF in its neutral state is shown in Figure 9 and for comparison is overlaid with spectra of P3HT, MEH-PPV, and PT34bT along with the solar flux under air mass 1.5 conditions (AM1.5-G; i.e., sunlight that passes through the atmosphere at 42° from horizon) and the absorption of crystalline silicon.[38] It is important to note that the *Y*-axis of Figure 9 is in energy units ($W/(m^2$ nm)) and corresponds to solar flux, while the absorption spectra of the organic materials were normalized to an arbitrary height, but the λ_{max} of the materials was not altered. Thus, the ordinate for the materials should be in normalized dimensionless absorbance scale, and the figure is accurate in terms of the wavelength, i.e. abscissa, where comparisons are made. It is clear that crystalline silicon has a broad absorption, and the currently used organic polymers suffer both in terms of absorption range and the location of the maximum: they have relatively sharp absorptions at the high-energy end. However, PT34bF exhibits broader absorptions and at lower energies – where the maximum number of photons are – and is a direct result of the low band gap of this material. Further, the absorption spectrum of PT34bF shows a remarkable matching to that of the crystalline silicon and therefore will have the ability to trap photons across the solar spectrum, including the low energy end, fitting the projected need for low band gap materials. The potential to use both PT34bF and P3HT (or other higher band gap materials), in tandem, will lead to improved light harvesting both in the low- and high-energy end of the solar spectrum.

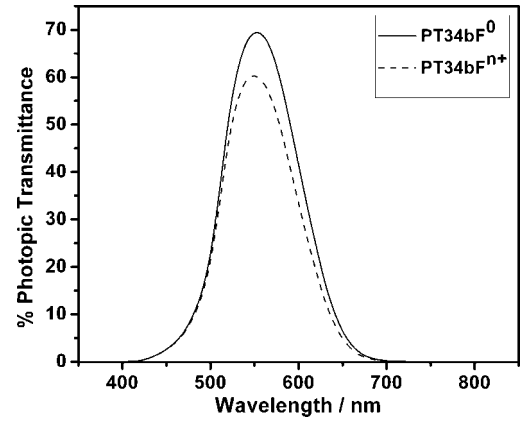

Figure 10. Photopic transmittance spectra of PT34bF in the oxidized state (+0.6 V, solid line) and neutral state (−0.6 V, dashed lines).

Photopic Transmission. For optically transparent applications, it is important to consider the photopic transmission values rather than the spectrum obtained from an instrument as the human eye, unlike a detector in a spectrophotometer, which has a different response across the visible spectrum and is the most sensitive at 555 nm. Thus, reporting the photopically weighted spectra of PT34bF in oxidized and neutral states is appropriate, and these values will be closer to what will be apparent by a human observer as a measure of optical transparency. To calculate the photopic values, eq 2 was used, and the photopically weighted spectra are plotted in Figure 10. In eq 2, $T(\lambda)$ corresponds to the spectral transmittance of the sample (PT34bF) under test, $S(\lambda)$ is the normalized spectral emittance of a 6000 K blackbody radiation, and $P(\lambda)$ is the normalized spectral response of the eye.

$$T_{\text{photopic}} = \frac{\int_{380}^{720} T(\lambda)\, S(\lambda)\, P(\lambda)\, d\lambda}{\int_{380}^{720} S(\lambda)\, P(\lambda)\, d\lambda} \qquad (2)$$

Transmittance of PT34bF at 715 nm (λ_{max}), 555 nm (most eye sensitive λ), and the photopically weighted spectrum showed similar values of 72% in the oxidized state. In the neutral state, PT34bF showed 62% transmittance when measured photopically while showing only 52% transmittance at λ_{max}. Thus, as perceived by the human eye, there is a drop of transmission from 72% to 62% upon switching the polymer from the oxidized to the neutral form.

Conductivity Measurements. Electrochemically polymerized PT34bF was pressed into a 1.2 cm diameter pellet and was used for conductivity measurement using a four-point collinear array. Five measurements varying in the applied current between 1×10^{-5} and 1×10^{-7} A were taken, and the measured potential changed linearly. The resistance values were found to be same (within 2% error), indicating Ohmic response. For the neutral form, a conductivity of 10^{-5} S/cm was calculated, and upon doping with iodine the conductivity increased to 10^{-2} S/cm. These values are similar to that of PT34bT obtained from dimer having 4,4′- and 6,6′-linkages.[39]

Density Functional Theory Calculation of Geometry and Band Structure of Polymer. Gaussian 03[29] with a periodic boundary conditions (PBC) routine[30] has been used in this study. Although the oligomer approach[40] has also been used to study properties of polymers, this method involves the gradual building of oligomers and optimizing them to fit the function of the HOMO and LUMO levels with that of oligomer size until

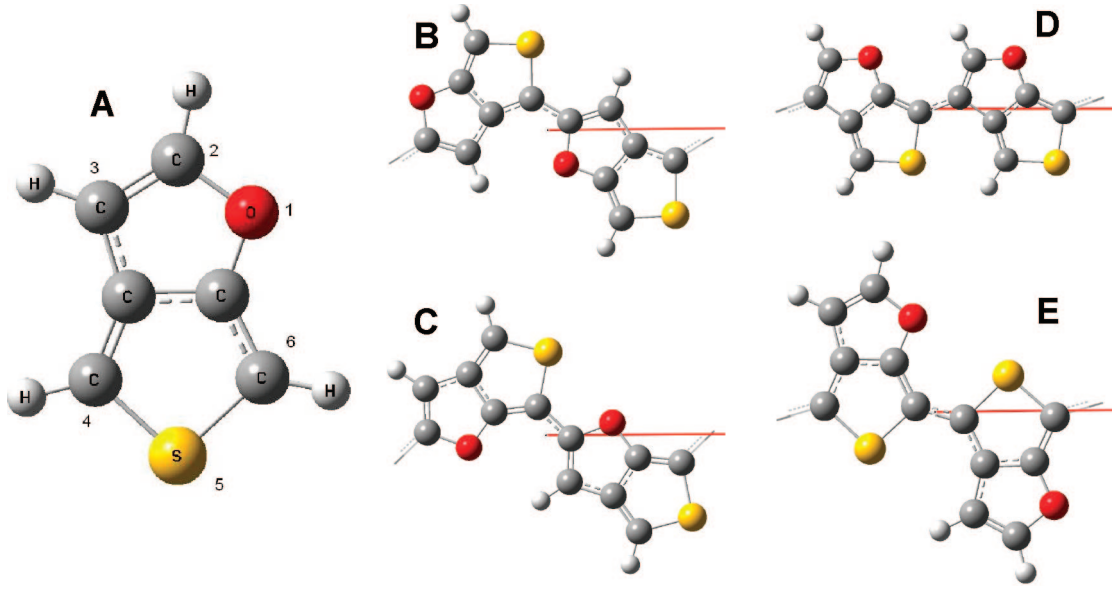

Figure 11. (a) Thieno[3,4-*b*]furan monomer and numbering of atomic positions; red = oxygen, yellow = sulfur atoms. The possible connectivities are through positions (b) 2−4, (c) 2−6, (d) 3−6, and (e) 4−6. The red horizontal lines represent the translational vector.

Table 2. Geometric and Band Properties for Different Connections in T34bF

connection	2−4	2−6	3−6	4−6
a (Å)	9.23	9.89	9.81	7.90
HOCO (eV)	−4.84	−5.31	−5.20	−3.92
BW (eV)	0.9	0.24	0.49	2.29
m^* (m_0)	−0.202	∞	−0.672	−0.067
LUCO (eV)	−2.72	−2.15	−1.88	−2.91
BW (eV)	1.36	0.54	0.49	2.04
m^* (m_0)	0.202	1.210	0.756	0.076
E_g (eV)	2.12	3.16	3.32	1.01

saturation is observed. As such, the computational cost of the oligomer approach is high with respect to PBC in which an infinite polymer chain is directly optimized using translational symmetry. In addition, PBC allows the investigation of band structure in the Brillouin zone. Several recent studies[41] have utilized the PBC routine of the Gaussian 03 program package to various polymers.

The monomer structure with atomic symbols and numbering is given in Figure 11a; connections of the polymers are given according to this numbering, and the optimized geometries of different connections are given in Figure 11b−e. Horizontal lines represent the translational vector which is equal to the one-dimensional cell size. Each cell must contain at least two monomers to fix connection sides. Intercell bond lengths and length of the bond connecting two monomers in the cell are the same for each connection, and their values are 1.43, 1.43, 1.45, and 1.42 in the order given in Figure 11, respectively, and comparing them with that of the neighboring bonds indicates increased single bond character. Therefore, polymers of different connections all have aromatic structure, and π-electrons are mostly localized on the rings rather than the bonds between the rings, keeping in mind that all the bonds through the conjugated backbone are neither a double nor single bond but are a hybrid of the two.

Cell parameter *a* is not the same for all the connections although all the same number of same type monomers are included (Table 2). This is clearly due to different geometrical arrangements of the monomers in the cell. It is noticeable that the 4−6 connectivity has the lowest band gap and also has the lowest cell parameter. Different positions of the same atoms in the different connections result in different band structure. The number of bonds through the C−C backbone in a cell is 10 for connection 2−6 and 8 for all others, considering that intercell bonds are shared between the two cells. The values of HOCO (highest occupied crystal orbital) and LUCO (lowest unoccupied crystal orbital) are also given in Table 2. (Note: HOCO corresponding to the experimental HOMO and LUCO in lieu of LUMO are justified as the values of the respective energy levels are calculated assuming a crystal lattice.) The reverse sign of these values can be used as a measure of the first ionization energy and first electron affinity of polymers, respectively, since energetically the electron in HOCO is the first one to be removed and the first electron to be injected will settle into the LUCO. These are values are important for p- and n-doping processes of the CP. As seen from Table 2, the lowest amount of energy will be required for oxidation of polymer with a 4−6 connection, and maximum energy is released for an electron injected into the polymer with the same connection. Thus, energetically, the polymer with the 4−6 connection is the most favorable one thermodynamically for both n- and p-doping. Further, since 4−6 connectivity has the lowest calculated band gap, it also has the highest number of electrons passing from the HOCO to the LUCO at a given temperature.

Electrical conductivity of the polymer depends on the mobility of a hole in the HOCO or an electron in LUCO, and mobility strongly depends on two parameters: bandwidth (BW) and effective mass (m^*). As the bandwidth increases the mobility also increases, and the highest bandwidth values of HOCO and LUCO bands are observed for the 4−6 connection, implying the highest mobility for a polymer with 4−6 connectivity compared to others. The effective mass is given with the following equation:[42]

$$\frac{1}{m^*} = \frac{1}{\hbar^2}\frac{\mathrm{d}^2E(k)}{\mathrm{d}k^2} \tag{3}$$

where m^* is the effective mass, $\hbar$ is the reduced Planck constant, and $E(k)$ is the energy as a function of k, the wave vector in the reciprocal space. Band structures in the positive region of first Brillouin zone (between $k = 0$ and π/a) for the different connections are given in Figure 12.

As seen from the figure, the lowest band gap values occur at Γ point ($k = 0$), suggesting that these are all direct band gap polymers. The second derivative in eq 3 is taken using the second-order polynomial equation fitted to the energy values

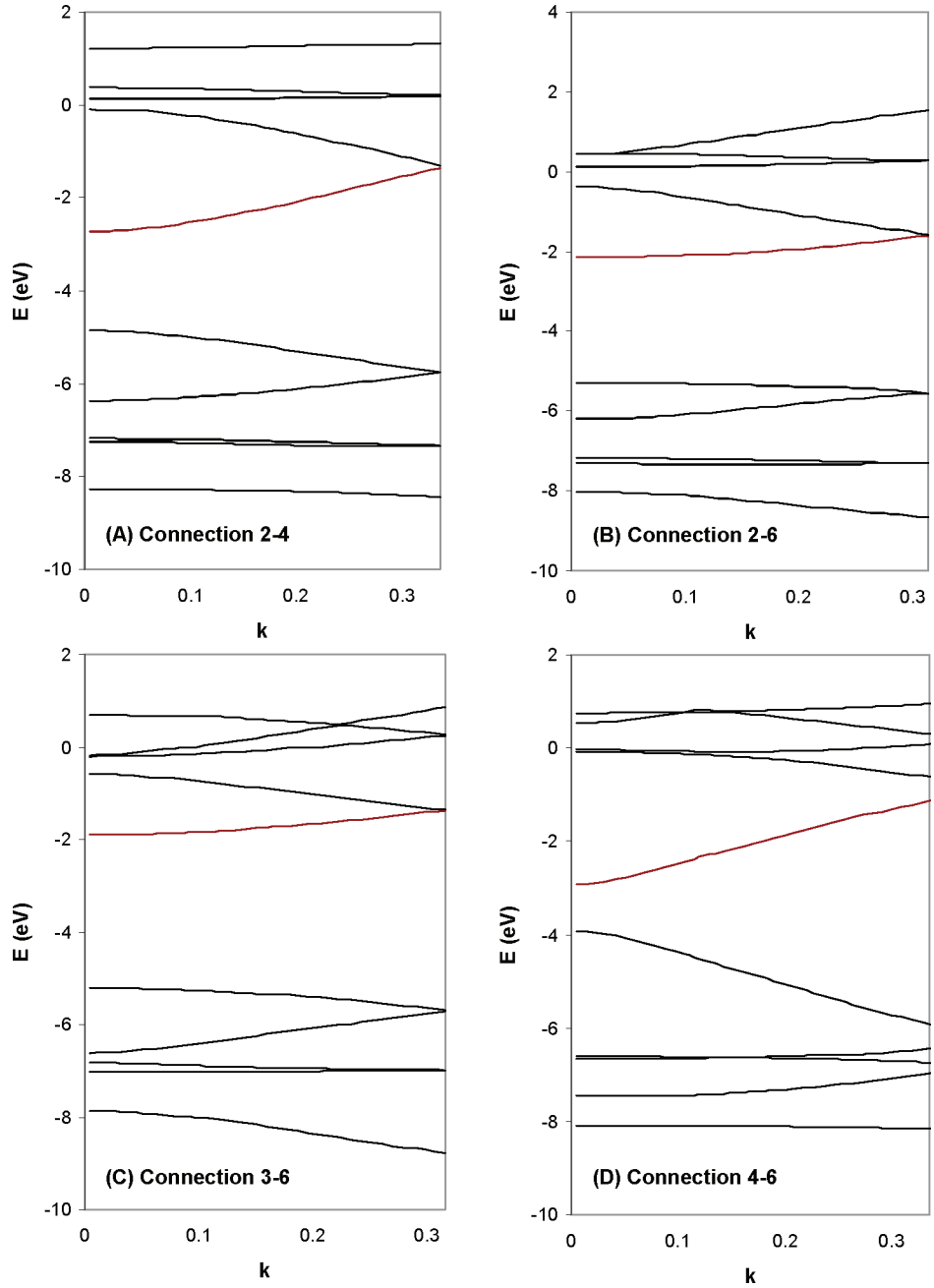

Figure 12. Band structures of PT34bF formed through the various connections in the positive region of first Brillouin zone (between $k = 0$ and π/a) for the different connections: (A) connection 2−4; (B) connection 2−6; (C) connection 3−6; (D) connection 4−6. The k values in abscissa are in $Å^{-1}$ units.

near the Γ point. It is clear that there is an inverse correlation between curvature and m^*, and the calculated effective mass values are given in terms of rest mass of electron (m_0) in Table 2. The effective mass value is found to be infinity for the HOCO of 2−6 connectivity since the band is almost flat with nearly zero curvature. This means that the mobility of an electron approaches zero in this band. The lowest effective mass is observed for both HOCO and LUCO of 4−6 connectivity. Thus, considering the effective mass, again the polymer with 4−6 connectivity has the highest mobility in both the valence and conduction band. Therefore, the polymer with connection 4−6 will display good conducting properties and will be the most favorable since it has the lowest ionization energy as compared to other connectivities that would also result in PT34bF. Calculations of the spin density distribution in T34bF radical was performed and the Mulliken atomic spin densities were 0.084, 0.156, 0.190, 0.466, −0.047, and 0.311 for atoms 1−6 as labeled in Figure 11a, respectively, where atom 1 is oxygen and 5 is sulfur. Taking spin population as a measure of reactivity, highest electron density on carbons 4 and 6 indicates that these positions are most reactive (relative to other positions), once again suggesting most probable formation of 4−6 connection in PT34bF.

Our calculated band gap value for the 4−6 connectivity is in excellent agreement with the experimentally obtained value and is in good agreement with the energies of the absolute energy levels (vide supra, Figure 5). However, there are two points that should be considered. First, the calculated band gap value obtained from the difference between the HOCO and LUCO does not correspond to the experimental value observed for the transition between the ground-state and first-dipole-allowed state. Some excited-state theories produce band gap values that are comparable with the experiment. However, the excitation energies for polymers predicted by TDDFT, one of the excited-

state theories, converge to about the same value as the HOCO−LUCO band gap at the same theoretical level within the errors and uncertainties of theoretical calculations,[43] and therefore comparison of theoretical HOCO−LUCO band gap value with the experimentally obtained value could be meaningful. Second, interchain interactions have not been taken into account, and calculations have been carried out for infinitely long one-dimensional chain. One calculation showed that this interaction causes a 0.2 eV reduction in the band gap value, and increasing the Hartree−Fock (HF) term in the functional results in broadening of the band gap. Therefore, band gap values could be adjusted with the Hartree−Fock term that corrects the interchain interaction, and results consistent with the experimental values can be obtained. It is emphasized, however, that in this study there was no need for such an adjustment, and no correction for the interchain interaction was applied: The default coefficient of the HF term was used. This is reasonable as the band gap value for the 4−6 connectivity was found to be in excellent agreement with the experimental value, and there is no reason or evidence to suspect that polymers having other connectivities would behave differently. Further, since the deviation of the experimental value from the calculated values of other connections far exceed the uncertainty involved in interchain interaction, it is negligible for the comparison of PT34bFs with different connectivities.

Conclusions

We have reported a more time- and cost-efficient, scalable procedure for the synthesis of T34bF monomer compared to that reported earlier in that purification is avoided until the last synthetic step. PT34bF shows stable redox behavior with anion dominant ion transport and upper limit of doping level at 30%. When neutralized at −0.6 V, PT34bF showed a λ_{max} at 1.73 eV (715 nm) and an E_g of 1.04 eV (1190 nm), which qualifies it as a low energy gap polymer. This value is similar to the reported value of 1.03 eV for chemically neutralized PT34bF.[27] PT34bF showed a photopic transmittance of 72% and 62% in the oxidized and neutral state, respectively, indicating little change in transparency level between redox states. Therefore, PT34bF could serve as an optically transparent ion- storage layer in electronic and optoelectronic devices. Taken together, the conductivity data, the optoelectrochemistry and the theoretical calculations very strongly point that the connectivity during polymerization of T34bF is predominantly between the positions α to the sulfur (4 and 6 positions) and that the 2 position (α to oxygen) for the most part is not involved in the polymerization. This implies that the 2 position is available for derivatization and therefore making possible to tune the electronic, optical, and solubility properties of PT34bF-based polymers. Attempts to make water-soluble PT34bF via ring sulfonation and organic-soluble PT34bF via attaching alkyl group to the ring are in progress and will be reported later. PT34bF has a great spectral match to the solar flux and to crystalline silicon. Furthermore, PT34bF exhibits appropriate band energies. With these two factors taken into consideration, PT34bF could serve well within the active layer of an organic photovoltaic.

Acknowledgment. G. Sotzing thanks the University of Connecticut and the National Science Foundation (CHE-0349121), and Z. Buyukmumcu thanks the Research Fund of Erciyes University for the financial support of this work.

References and Notes

(1) (a) Chiang, C. K.; Fincher, C. R., Jr.; Park, Y. W.; Heeger, A. J.; Shirakawa, H.; Louis, E. J.; Gau, S. C.; MacDiarmid, A. G. *Phys. Rev. Lett.* **1977**, *39*, 1098. (b) Shirakawa, H.; Louis, E. J.; MacDiarmid, A. G.; Chiang, C. K.; Heeger, A. J. *J. Chem. Soc., Chem. Commun.* **1977**, *16*, 578.

(2) (a) Schwendeman, I.; Hwang, J.; Welsh, D. M.; Tanner, D. B.; Reynolds, J. R. *Adv. Mater.* **2001**, *13*, 634. (b) Schottland, P.; Zong, K.; Gaupp, C. L.; Thompson, B. C.; Thomas, C. A.; Giurgiu, I.; Hickman, R.; Abboud, K. A.; Reynolds, J. R. *Macromolecules* **2000**, *33*, 7051. (c) Thompson, B. C.; Schottland, P.; Zong, K.; Reynolds, J. R. *Chem. Mater.* **2000**, *12*, 1563.

(3) (a) McQuade, D. T.; Pullen, A. E.; Swager, T. M. *Chem. Rev.* **2000**, *100*, 2537. (b) Yang, J.-S.; Swager, T. M. *J. Am. Chem. Soc.* **1998**, *120*, 11864. (c) Sotzing, G. A.; Briglin, S.; Grubbs, R. H.; Lewis, N. S. *Anal. Chem.* **2000**, *72*, 3181.

(4) Ma, H.; Chen, B.; Sassa, T.; Dalton, L. R.; Jen, A. K.-Y. *J. Am. Chem. Soc.* **2001**, *123*, 986.

(5) Yu, G.; Heeger, A. J. *Synth. Met.* **1997**, *85*, 1183.

(6) Ferraris, J. P.; Eissa, M. M.; Brotherston, I. D.; Loveday, D. C. *Chem. Mater.* **1998**, *11*, 3528.

(7) Jonas, F.; Heywang, G. *Electrochim. Acta* **1994**, *39*, 1345.

(8) Perucki, M.; Chandrasekhar, P. *Synth. Met.* **2001**, *119*, 385.

(9) (a) Brabec, C. J.; Sariciftci, N. S.; Hummelen, J. C. *Adv. Funct. Mater.* **2001**, *11*, 15. (b) Henckens, A.; Knipper, M.; Polec, I.; Manca, J.; Lutsen, L.; Vanderzande, D. *Thin Solid Films* **2004**, *451−452*, 572.

(10) (a) Gross, M.; Muller, D. C.; Nothofer, H.-G.; Scherf, U.; Neher, D.; Brauchle, C.; Merrholz, K. *Nature (London)* **2000**, *405*, 661. (b) Book, K.; Bässler, H.; Elschner, A.; Kirchmeyer, S. *Org. Electron.* **2003**, *4*, 227.

(11) Pomerantz, M. In *Handbook of Conducting Polymers*, 2nd ed.; Skotheim, A., Elsenbaumer, R., Reynolds, J., Eds.; Marcel Dekker: New York, 1998; p 277.

(12) (a) Schwendeman, I.; Hwang, J.; Welsh, D. M.; Tanner, D. B.; Reynolds, J. R. *Adv. Mater.* **2001**, *13*, 634. (b) Sonmez, G.; Sonmez, H. B.; Shen, C. K. F.; Wudl, F. *Adv. Mater.* **2004**, *16*, 1905. (c) Argun, A. A.; Aubert, P.-H.; Thompson, B. C.; Schwendeman, I.; Gaupp, C. L.; Hwang, J.; Pinto, N. J.; Tanner, D. B.; MacDiarmid, A. G.; Reynolds, J. R. *Chem. Mater.* **2004**, *16*, 4401.

(13) (a) Sonmez, G.; Meng, H.; Wudl, F. *Chem. Mater.* **2003**, *15*, 4923. (b) Meng, H.; Tucker, D.; Chaffins, S.; Chen, Y.; Helgeson, R.; Dunn, B.; Wudl, F. *Adv. Mater.* **2003**, *15*, 146. (c) Chandrasekhar, P.; Birur, G. C.; Stevens, P.; Rawel, S.; Pierson, E. A.; Miller, K., L. *Synth. Met.* **2001**, *119*, 293.

(14) (a) Yao, Y.; Liang, Y.; Shrotriya, V.; Xiao, S.; Yu, L.; Yang, Y. *Adv. Mater.* **2007**, *19*, 3979.

(15) (a) Chen, M. X.; Perzon, E.; Robisson, N.; Joensson, S. K. M.; Andersson, M. R.; Fahlman, M.; Berggren, M. *Synth. Met.* **2004**, *146*, 233. (b) Brabec, C. J.; Winder, C.; Sariciftci, N. S.; Hummelen, J. C.; Dhanabalan, A.; Van, H.; Paul, A.; Janssen, R. A. J. *Adv. Funct. Mater.* **2002**, *12*, 709.

(16) Kiebooms, R. H. L.; Goto, H.; Akagi, K. *Macromolecules* **2001**, *34*, 7989.

(17) Wudl, F.; Kobayashi, M.; Heeger, A. J. *J. Org. Chem.* **1984**, *49*, 3382.

(18) (a) Kobayashi, M.; Colaneri, N.; Boysel, M.; Wudl, F.; Heeger, A. J. *J. Chem. Phys.* **1985**, *82*, 5717. (b) Colerneri, N.; Kobayashi, M.; Heeger, A. J.; Wudl, F. *Synth. Met.* **1986**, *14*, 45.

(19) (a) van Asselt, R.; Vanderzande, D.; Gelan, J.; Froehling, P. E.; Aagaard, O. *Synth. Met.* **2000**, *110*, 25. (b) Kisselev, R.; Thelakkat, M. *Macromolecules* **2004**, *37*, 8951. (c) Goris, L.; Loi, M. A.; Cravino, A.; Neugebauer, H.; Sariciftci, N. S.; Polec, I.; Lutsen, L.; Andries, E.; Manca, J.; De Schepper, L.; Vanderzande, D. *Synth. Met.* **2003**, *138*, 249.

(20) (a) Meng, H.; Wudl, F. *Macromolecules* **2001**, *34*, 1810. (b) Cravino, A.; Loi, M. A.; Scharber, M. C.; Winder, C.; Neugebauer, H.; Denk, P.; Meng, H.; Chen, Y.; Wudl, F.; Sariciftci, N. S. *Synth. Met.* **2003**, *137*, 1435.

(21) Pomerantz, M.; Gu, X.; Zhang, S. X. *Macromolecules* **2001**, *34*, 1817.

(22) Neef, C. J.; Brotherston, I. D.; Ferraris, J. P. *Chem. Mater.* **1999**, *11*, 1957.

(23) (a) Lee, K.; Sotzing, G. A. *Macromolecules* **2001**, *34*, 5746. (b) Lee, K.; Sotzing, G. A. *Macromolecules* **2002**, *35*, 7281.

(24) Lee, B.; Seshadri, V.; Sotzing, G. A. *Langmuir* **2005**, *21*, 10797.

(25) Lee, B.; Seshadri, V.; Sotzing, G. A. *Adv. Mater.* **2005**, *17*, 1792.

(26) Seshadri, V.; Lu, W.; Sotzing, G. A. *Langmuir* **2003**, *19*, 9479.

(27) Kumar, A.; Buyukmumcu, Z.; Sotzing, G. A. *Macromolecules* **2006**, *39*, 2723.

(28) Suen, Y. F.; Hope, H.; Nantz, M. H.; Haddadin, M. J.; Kurth, M. J. *J. Org. Chem.* **2005**, *70*, 8468.

(29) Frisch, M. J.; Trucks, G. W.; Schlegel, H. B.; Scuseria, G. E.; Robb, M. A.; Cheeseman, J. R.; Montgomery, Jr., J. A.; Vreven, T. Kudin, K. N.; Burant, J. C.; Millam, J. M.; Iyengar, S. S.; Tomasi, J.; Barone, V.; Mennucci, B.; Cossi, M.; Scalmani, G.; Rega, N.; Petersson, G. A.; Nakatsuji, H.; Hada, M.; Ehara, M.; Toyota, K.; Fukuda, R.; Hasegawa, J.; Ishida, M.; Nakajima, T.; Honda, Y.; Kitao, O.; Nakai, H.; Klene, M.; Li, X.; Knox, J. E.; Hratchian, H. P.; Cross, J. B.; Adamo, C.; Jaramillo, J. R.; Gomperts, R. E.; Stratmann, O.; Yazyev, A. J.; Austin, R.; Cammi, C.; Pomelli, J. W.; Ochterski, P. Y.; Ayala, K.; Morokuma, G. A.; Voth, P.; Salvador, J. J.; Dannenberg, V. G.; Zakrzewski, S.;

Dapprich, A. D.; Daniels, M. C.; Strain, O.; Farkas, D. K.; Malick, A. D.; Rabuck, K.; Raghavachari, J. B.; Foresman, J. V.; Ortiz, Q.; Cui, A. G.; Baboul, S.; Clifford, J.; Cioslowski, B. B.; Stefanov, G.; Liu, A.; Liashenko, P.; Piskorz, I.; Komaromi, R. L.; Martin, D. J.; Fox, T.; Keith, M. A.; Al-Laham, Peng, C. Y.; Nanayakkara, A.; Challacombe, M.; Gill, P. M. W.; Johnson, B.; Chen, W.; Wong, M. W.; Gonzalez, C.; Pople, J. A. Gaussian 03, Revision C.02, Gaussian, Inc., Wallingford, CT, 2004.

(30) Kudin, K. N.; Scuseria, G. E. *Phys. Rev. B* **2000**, *61*, 16440.

(31) Perdew, J. P.; Burke, K.; Wang, Y. *Phys. Rev. B* **1996**, *54*, 16533.

(32) Moursounidis, J.; Wege, D. *Tetrahedron Lett.* **1986**, *27*, 3045.

(33) Groenendaal, L.; Zotti, G.; Aubert, P.; Waybright, S. M.; Reynolds, J. R. *Adv. Mater.* **2003**, *15*, 855.

(34) Bokria, J. G.; Kumar, A.; Seshadri, V.; Tran, A.; Sotzing, G. A. *Adv. Mater.* **2008**, *20*, 1175.

(35) (a) Khan, T.; Mcdouall, J. W.; Mcinnes, E. J. L.; Skabara, P. J.; Frere, P.; Coles, S. J.; Hursthouse, M. B. *J. Mater. Chem.* **2003**, *13*, 2490. (b) Biswas, P. K.; De, A.; Dua, L. K.; Chkoda, L. *Appl. Surf. Sci.* **2006**, *253*, 1953. (c) Osada, T.; Kugler, Th.; Bröms, P.; Salaneck, W. R. *Synth. Met.* **1998**, *96*, 77.

(36) (a) Milliron, D. J.; Hill, I. G.; Shen, C.; Kahn, A.; Schwartz, J. *J. Appl. Phys.* **2000**, *87*, 572. (b) Sugiyama, K.; Ishii, H.; Ouchi, Y.; Seki, K. *J. Appl. Phys.* **2000**, *87*, 295. (c) Andreasson, M.; Tengelin-Nilsson, M.; Andersson, T. G.; Ilver, L.; Kanski, J. *Org. Electron.* **2005**, *6*, 175.

(37) Berlin, A.; Schiavon, G.; Zecchin, S.; Zotti, G. *Synth. Met.* **2001**, *119*, 153.

(38) Internet: http://www.vicphysics.org/documents/events/stav2005/spectrum JPG (accessed Nov 12, 2007).

(39) Lee, B.; Yavuz, M. S.; Sotzing, G. A. *Macromolecules* **2006**, *39*, 3118.

(40) (a) Salzner, U. *Curr. Org. Chem.* **2004**, *8*, 569. (b) Salzner, U.; Lagowski, J. B.; Pickup, P. G.; Poirier, R. A. *Synth. Met.* **1998**, *96*, 177. (c) Hutchison, G. R.; Zhao, Y. J.; Delley, B.; Freeman, A. J.; Ratner, M. A.; Marks, T. J. *Phys. Rev. B* **2003**, *68*, 035204. (d) Salzner, U. *J. Phys. Chem. B* **2002**, *106*, 9214. (e) Salzner, U.; Kose, M. E. *J. Phys. Chem. B* **2002**, *106*, 9221.

(41) (a) Bartha, F.; Howard, I. A.; Geerlings, P.; Alsenoy, C. V.; Vanderzande, D.; Cleij, T. J.; Bogar, F. *Int. J. Quantum Chem.* **2006**, *106*, 1912. (b) Liu, C. L.; Tsai, F. C.; Chang, C. C.; Hsieha, K. H.; Lin, J. L.; Chen, W. C. *Polymer* **2005**, *46*, 4950. (c) Pai, C. L.; Liu, C. L.; Chen, W. C.; Jenekhe, S. A. *Polymer* **2006**, *47*, 699. (d) Tsai, F. C.; Chang, C. C.; Liu, C. L.; Chen, W. C.; Jenekhe, S. A. *Macromolecules* **2005**, *38*, 1958.

(42) Kittel, C. *Introduction to Solid State Physics*; John Wiley & Sons: New York, 1996.

(43) Yang, S.; Kertesz, M. *J. Phys. Chem. A* **2006**, *110*, 9771, and references therein.

MA702773E